Advanced Optical Materials

ADVANCED OPTICAL MATERIALS
www.advopticalmat.de

RESEARCH ARTICLE

Impact of Molecular Contortion on Photophysics and Photostability in Functionalized Pentacenes

Karl J. Thorley[1] | Aisha Shakir[2] | Avneesh Kudrimoti[3] | Sean R. Parkin[2] | Shahnawaz R. Rather[2] | John E. Anthony[1,2]

[1]Center for Applied Energy Research, University of Kentucky, Lexington, Kentucky, USA | [2]Department of Chemistry, University of Kentucky, Lexington, Kentucky, USA | [3]Paul Laurence Dunbar High School, Lexington, Kentucky, USA

Correspondence: Karl J. Thorley (karl.thorley@uky.edu)

Received: 30 March 2026 | **Revised:** 30 July 2026 | **Accepted:** 6 August 2026

Keywords: acenes | molecular contortion | non-radiative decay | photostability | transient absorption

ABSTRACT

Functionalized acenes are of interest for photonics applications, including singlet fission-enhanced solar energy. In this work, we study the photophysics of a pentacene derivative that features a contorted structure due to the interactions of solubilizing side chains, and compare it to an isomeric pentacene with similar functional groups but lacking the core twisting feature. Density functional theory calculations are used to establish the impact of core torsion and functional group contributions to the optical properties of the acenes. Transient absorption spectroscopy identifies short excited-state lifetimes in solution that contribute to enhanced photostability of the contorted pentacene.

1 | Introduction

Acenes are a class of polycyclic aromatic hydrocarbon that have been widely studied for their opto-electronic properties and photonics applications [1–6]. The acene structure consists of linearly fused benzenoid rings, where any given closed shell resonance form contains only a single Clar sextet [7]. The visible absorption shows a steady 100 nm red-shift upon elongating this acene structure [8], giving access to materials that can be tailor-made to absorb light of specific wavelengths. Most acenes show strong fluorescence ($ø_{fl}$ up to 80%), with small Stokes shifts of 10 nm indicating very little structural reorganization in the excited state [9]. Introduction of functional groups at various positions around the periphery can be utilized to further fine-tune these basic optical properties [6, 10].

A large amount of recent research has looked at singlet fission [11] processes in acenes [12–16], which is possible due to the low triplet energy of these materials, in part due to increasing ground-state diradical character with acene length [17]. The triplet energies of tetracene and pentacene lie around halfway between the ground and first excited singlet states [18], meaning that after light absorption and occupation of the S_1 state, a correlated triplet pair (TT) of overall singlet multiplicity state can form across two adjacent molecules which eventually can be split into two distinct triplet states [19–21]. This process has great potential in solar energy, where a light-harvesting and multiplication layer might be added to existing silicon photovoltaic technologies [22–25]. The acene layer can better utilize the mid-visible light spectrum, generating two charge carriers per absorbed photon while also reducing heat losses. Other applications of singlet fission materials rely on the optical generation of entangled triplet pairs, which can be manipulated to different spin states for use in quantum computing [26–28]. These singlet fission applications require a thorough understanding of the optical properties of acenes.

We recently reported on the synthesis and transistor performance of some rather unusual acene derivatives, namely TIPS-PhPN (Figure 1) which bears a combination of silylethynyl groups which

All rights reserved, including rights for text and data mining and training of artificial intelligence technologies or similar technologies.
© 2026 Wiley-VCH GmbH

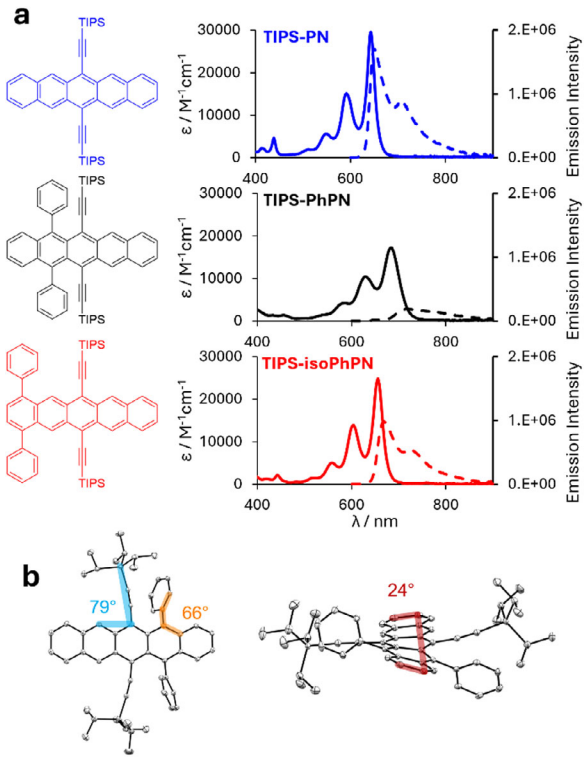

FIGURE 1 | (a) Chemical structures of TIPS-PN, TIPS-PhPN, and TIPS-isoPhPN and absorption (solid) and emission (dashed) spectra recorded in $CHCl_3$ at 298 K. Emission spectra were collected with the same absorbance at the excitation wavelength (590 nm). TIPS = tri-isopropylsilyl. (b) Alkyne bend (blue), aryl torsion (orange) and pentacene twist (red) in the X-Ray crystal structure of TIPS-PhPN [29].

are commonplace in many derivatives due to their solubilizing and stabilizing properties, and phenyl groups intended to act as dampers to minimize molecular displacements in the solid-state [29]. The interaction between these two different side chains within the same molecule induced a twisting of the pentacene cores, altering the conjugation within the acene structure and therefore affecting the opto-electronic properties. These materials exhibited red-shifted and broadened UV–vis absorption spectra (Figure 1a), indicative of electronic effects between the pentacene and phenyl rings and of the conformational fluctuation of the acene core. These properties were comparable to previously reported tetracenes with similar functional groups [30], but while those tetracenes retained high fluorescence quantum yield (75%), our recent pentacenes were only weakly emissive. Rubrene possesses a similarly twisted structure in the gas phase and has fluorescence quantum yields up to 96% in solution [31]. Other work has used covalent tethers to produce static twisted anthracene or pentacene [32] cores, although this approach blocks intermolecular interactions in the solid-state, which can limit applications of these materials. Diminished fluorescence in twisted anthracenes has been assigned to increased spin-orbit coupling, which accelerates intersystem crossing and non-emissive triplet yield [33]. An array of larger contorted polycyclic aromatics such as perylene bisimides [34, 35], nanographenes [36–38], and helicenes [39–42] have been reported. The rather unusual optical properties of our previous contorted pentacenes led us to investigate in more detail their electronic and geometric structure. This has been achieved through a combination of computational modeling using density functional theory (DFT), the synthesis of a new pentacene derivative (TIPS-isoPhPN, Figure 1a) to act as a reference material, followed by thorough time-resolved transient absorption spectroscopic analysis to deduce the effect of pentacene contortion on their optical properties.

2 | Results and Discussion

2.1 | Steady-State Spectroscopy

To investigate the contributions of functional groups on the optical properties through experimental methods, an isomer of TIPS-PhPN bearing the phenyl substituents on the terminal pentacene rings (TIPS-isoPhPN) was synthesized as outlined in the Supporting Information. Relocating the phenyl groups to the outer pentacene rings removes the steric constraints from the middle of the molecule, resulting in a material that possesses a planar acene core and unperturbed alkynyl functional groups. These structural features were confirmed by DFT geometry optimization (Figure S29) as well as single crystal X-Ray diffraction (Table S1). The inductive or resonance contributions of the phenyl groups are still present, and dynamic rotation of the phenyl groups might still contribute to opto-electronic properties. From UV–vis measurements, the lowest energy excitation at 656 nm is red-shifted from TIPS-PN (643 nm) but not as far as TIPS-PhPN (685 nm). These shifts provide an indication of the strength of the inductive effect of the phenyl groups. However, it has already been noted that the substituent position on an acene can affect the magnitude of the electronic effects of the substituent, according to the relative distribution of the HOMO and the LUMO across different substitution sites [10]. The absorption spectrum of TIPS-isoPhPN is similar to the 2,9-diaryl TIPS-PN derivatives that have been previously reported [43].

Another notable feature in the UV–vis spectra of the three pentacene derivatives is difference in the broadening of the absorption band, provided in Table 1 as the half-width at half-maximum (HWHM) measured on the low-energy side of the lowest excitation. TIPS-PhPN exhibits the broadest absorption, with HWHM of 374 cm^{-1}, and an S_0-S_1 absorption band that spans 500–750 nm range. This broadening leads to a noticeable decrease in the extinction coefficient for TIPS-PhPN in comparison to TIPS-PN. TIPS-isoPhPN is more similar in its absorption properties to TIPS-PN than TIPS-PhPN, with a slight red-shifted maximum, slightly reduced extinction coefficient, and slight broadening. This indicates that simply adding the phenyl groups has a relatively minor effect and that the pentacene core torsion is responsible in some way for the further red-shifting and spectral broadening. There is little influence on the absorption properties of all materials by measuring in different solvents (Figures S11–S13), indicating a lack of charge-transfer type excitations. A decrease in the vibronic spacing in the series TIPS-PN>TIPS-isoPhPN>TIPS-PhPN reflects the change in vibrational energies of the ground and excited states upon distorting the planar geometry and bending of the alkynyl groups.

A large mystery from the initial study of these molecules was the lack of fluorescence, whereas similarly substituted tetracenes were strongly emissive [30]. While TIPS-PN showed a

TABLE 1 | Summary of steady-state optical properties of TIPS-PN, TIPS-PhPN and TIPS-isoPhPN measured in $CHCl_3$. [a] measured in air-equilibrated solvent and in parenthesis in freeze-pump-thaw degassed solvent. Data for other solvents provided in Supporting Information.

	$\lambda_{max(abs)}$ (nm)	ε ($M^{-1}cm^{-1}$)	HWHM (cm^{-1})	Vib. spacing (cm^{-1})	$\lambda_{max(fl)}$ (nm)	$ø_f$ [a]
TIPS-PN	643	29400	225	1341	651	0.36 (0.59)
TIPS-PhPN	685	16500	374	1300	716	0.08 (0.08)
TIPS-isoPhPN	656	24800	274	1312	670	0.27 (0.47)

fluorescence quantum yield of 0.36 in chloroform, this value drops to only 0.08 for TIPS-PhPN, accompanied by a loss of vibronic structure to the emission band. The fluorescence quantum yield of TIPS-isoPhPN is more similar to TIPS-PN, with a slight drop to 0.27, but this similarity indicates the mere presence of the phenyl groups is not the source of the diminished emission in TIPS-PhPN. Instead, it is more likely the core twisting contributes to altering the excited-state dynamics of this system to pathways alternative to fluorescence. Notably, the removal of oxygen from the solvent causes an increase in fluorescence quantum yield for TIPS-PN and TIPS-isoPhPN but does not alter the measured quantum yield of 0.08 for TIPS-PhPN, indicating that the TIPS-PhPN excited states are not being quenched by oxygen. Measurements in other solvents yielded similar trends (Tables S2 and S3).

For all three pentacenes, the excitation spectra (Figure S17) match well with the absorbance spectra, indicating higher excited states decay to the lowest energy singlet state before emission. The Stokes shift of the phenyl substituted pentacenes rises from that of the parent TIPS-PN (8 nm) to 14 nm (TIPS-isoPhPN) and further to 31 nm (TIPS-PhPN), indicating larger reorganization energies, which were confirmed by DFT calculations (λ_{opt} = 0.29 eV for TIPS-PN, 0.33 eV for TIPS-PhPN, 0.33 eV for TIPS-isoPhPN). While the Stokes shift taken from the absorbance and emission peaks is larger for TIPS-PhPN, the degree of overlap between the absorbance and emission is large due to the increased broadness of both absorption and emission spectra.

One reason for the lack of fluorescence might be the formation of triplet states. While singlet fission is energetically favorable based on computed excited state energies (similar to TIPS-PN), it is unlikely that this multichromophoric process occurs in such dilute samples as used for quantum yield determination. Other research groups have shown that PAH contortion can increase triplet yields by spin-orbit coupling (SOC). Houk et al. showed that twisting of a pentacene increases SOC [44], and experimental structures with twisted acene cores show diminished fluorescence quantum yield attributed to this effect [33, 45]. In those cases, the extreme steric repulsion or the tethering that induces the core distortion also make for a rather static system, which is different to TIPS-PhPN which is not tethered so has a more flexible structure.

SOC was computed for the minimum energy structures of the three pentacenes (Tables S4–S6), and while there is an increase in SOC by two orders of magnitude going from TIPS-PN (0.0012 meV) to TIPS-PhPN (0.12 meV), these values are still small compared to, e.g. heavy atom effects. Computed SOC values for TIPS-isoPhPN are similar to TIPS-PhPN, indicating that the origin of the modest SOC is the inclusion of the phenyl groups rather than the core twisting, and that significant triplet population is most likely not the reason for the low emission efficiency of TIPS-PhPN.

2.2 | Computational Modeling

Next, a range of DFT structures have been constructed to determine the origin of the red-shift in absorption and emission. The TIPS-PhPN structure has three main points of interest versus the parent TIPS-PN structure, namely the pentacene core twist, the phenyl group torsion relative to the pentacene core, and the bending of the ethynyl group to accommodate the additional phenyl groups. Based on simplified model structures, potential energy surfaces for pentacene core twisting, alkynyl bending, and phenyl rotation were computed by constrained geometry relaxation, and at each angle/torsion time-dependent DFT was carried out to gain S_0-S_1 excitation energies as a function of these geometric variations (Figures S18–S20).

Taken in isolation, the spectral shifts expected from each of the three effects is quite minor in comparison to the range of motion that might be expected in these model systems. Thermally accessible core twists of unsubstituted pentacene are in the region of ± 20° (Figure S18). The lowest energy excitation varies relatively little over this range of motion, with a red-shift of only 1 nm being predicted by TD-DFT for a 20° twist, and only a shift of 7 nm upon even further core twisting to 60°. The potential energy surface for alkynyl bending in model TIPS-PN structure (Figure S19) is steep, indicating this bend is energetically very unfavorable, although this does bring a larger influence on excitation energies. The PES for phenyl ring torsion in diphenyl pentacene (Figure S20) is much flatter, with accessible angles ± 40°, which also brings a more sizeable red-shift in absorbance of 10 nm.

However, in the TIPS-PhPN molecule all three effects are present simultaneously. The PES for each of the core twist, the alkyne bend, and the aryl torsion become dependent on one another, and so energetically disfavored twists become more favorable in the context of the whole molecule (Figure 2a). The optimal pentacene core twist in TIPS-PhPN gas-phase DFT PES is 30 °, close to the observed torsion in the experimental X-ray crystal structure (24 °) [29]. Moreover, the torsional PES of TIPS-PhPN is extremely shallow, allowing an even wider range of torsional angles than an unsubstituted acene – TIPS-PhPN core twist can freely fluctuate between 0 and 60° due to thermal energy at room temperature (Boltzmann distribution, Figure 2b). The torsional PES for TIPS-isoPhPN appears very similar to TIPS-PN due to

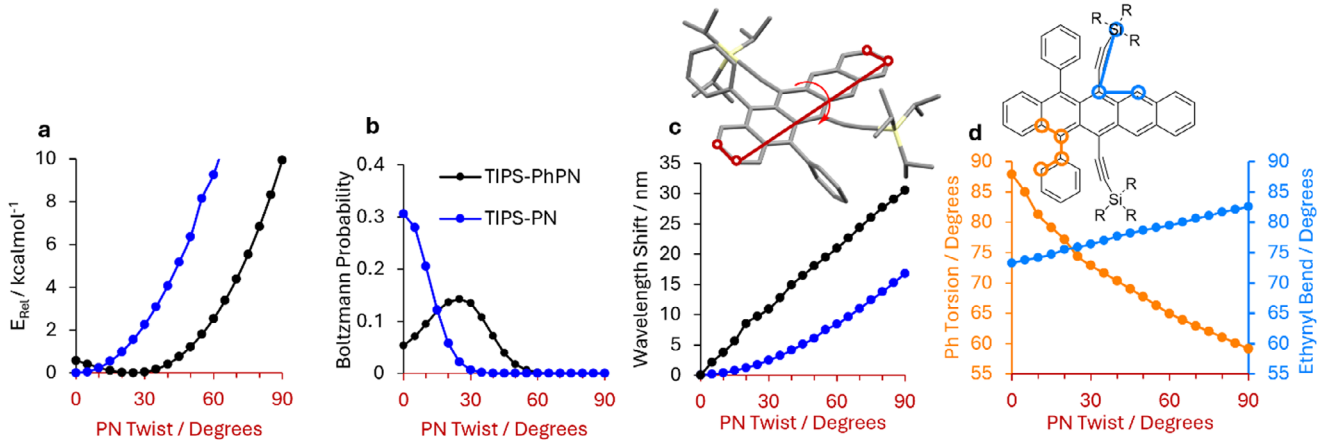

FIGURE 2 | (a) DFT (ωB97XD/6-31G*) potential energy surfaces for pentacene twisting in TIPS-PN (blue) and TIPS-PhPN (black) structures. (b) Boltzmann distribution of pentacene core twisting in TIPS-PN (blue) and TIPS-PhPN (black) at 298 K. (c) Associated shifts in computed S_0-S_1 wavelength of TIPS-PN (blue) and TIPS-PhPN (black) upon core twisting. (d) Dependence of aryl twisting (orange) and ethynyl bending (blue) on the pentacene core twist in TIPS-PhPN.

the lack of interaction between the phenyl and TIPS groups (Figure S21).

The alkyne bend (measured as the angle between the acene long-axis and the TIPS silicon atom as defined in Figure 2d) is 79 ° in the single crystal, while the aryl-pentacene torsion is 66 °. The interplay of the functional group interactions is evident in two ways; the pentacene contortion PES is shallower for TIPS-PhPN than for TIPS-PN (and TIPS-isoPhPN), but the effects on red-shifting the excitation energy are also stronger than the model systems (Figure 2c) since the twist of the pentacene core also induces a bend in the alkyne and a twist of the phenyl group (Figure 2d).

To investigate the roles of the phenyl and silylethynyl groups on the shallowing of the TIPS-PhPN torsional PES, we employed symmetry adapted perturbation theory (SAPT0) to look at the noncovalent interactions between these functional groups within the same molecule (Figures S23 and S24). To do this, the C—C bonds between the functional groups and the pentacene core were broken and the groups capped with hydrogen atoms to retain neutral spin-paired fragments. These separated Ph and TIPS-acetylene molecules were then used to determine the through-space interaction energies as a function of pentacene torsional angle. At low pentacene distortions, the interaction between Ph and TIPS groups is slightly repulsive. As the core becomes more twisted (up to 90°), the distance between the center of the Ph ring and the silicon atom of the TIPS group increases, but by less than 0.2 Å (Figure S23). Over this range, the repulsion between the groups diminishes and becomes slightly attractive at the most extreme core twist angles. Energy decomposition in the SAPT0 framework reveals that the major contribution to the change in non-covalent interaction energies is from reduced exchange repulsion (steric repulsion) stemming from the slight increase in functional group distance, while the changes in the attractive electrostatics, induction, and dispersion are more minor (Figure S24). Of course, these interactions probed by SAPT are purely through-space, but the changes in phenyl torsion and alkynyl bending also affect the energy of the pentacene core by changes in resonance.

As noted, the distance between Ph and Si stays about the same upon core twisting, with a slight decrease in repulsion by SAPT. This means that a completely flat pentacene core in TIPS-PhPN has an orthogonal Ph group and the largest alkyne bend (small angle as defined in Figure 2d). As the core twists, the Ph group rotates relative to the pentacene core as it maintains the non-covalent interaction with the neighboring TIPS group (Figure 2d). This also alleviates some of the strain on the alkyne bond, decreasing the bond bending (increasing the defined angle). Both of these effects add resonance stabilization to counteract the energy loss of twisting the pentacene core. Natural bond orbital analysis (Figure S25) reveals the extent of these delocalization effects. While the alkyne participates in resonance with the pentacene strongly (c.a. 20 kcal/mol), the changes in bending have a minimal effect on this delocalization energy (changes of less than 0.5 kcal/mol). Instead, the major changes in delocalization during the pentacene contortion come from increasing orbital overlap between pentacene and phenyl groups, which range between 0 and 5 kcal/mol depending on pentacene twist angle. By systematically removing the phenyl or TIPS-ethynyl groups from the optimized structures of the torsional PES and computing excitation energies without relaxation (Figure S26), the increased delocalization that comes with phenyl planarization is seen as the largest contributor to the red-shifted absorption in TIPS-PhPN.

With the origin of the red-shifted absorption resolved, the other aspect of TIPS-PhPN absorption spectrum can be addressed, which is the broadened absorption band with decreased intensity. The shallow torsional PES indicates a wider range of thermally accessible geometries due to the twisting motion, with Boltzmann distributions (Figure 2b) showing that while TIPS-PN can adopt core twists up to 30 °, TIPS-PhPN has more variability with twists between 0 and 60 °. Coupled with the increased wavelength shift for this twisting motion induced by the delocalization onto phenyl rings, this results in a wider range of excitation energies, and hence the broader S_0-S_1 absorbance band. The torsional PES of the S_1 state of TIPS-PhPN is similarly as broad as the ground state (Figure S22), indicating that the large range of core twisted geometries are also accessible in the excited state which is likely the largest contributor to the diminished fluorescence

due to competing non-radiative decay based around this core fluctuation.

2.3 | Ultrafast Excited State Dynamics

Ultrafast laser spectroscopy was employed to investigate the excited-state dynamics of the contorted pentacenes. Time-resolved transient absorption (TA) spectroscopy, covering a waiting-time window from femtoseconds to microseconds and probe spectral range from ~ 400 to 1500 nm, enables mapping of complete electronic population dynamics from the Franck–Condon state back to the ground state.

2.3.1 | Population Dynamics of TIPS-PhPN

Following the photo-excitation of TIPS-PhPN in tetrahydrofuran (THF) solvent (0.32 mM) at 670 nm with 0.2 μJ pulse energy, which promotes an electron to the lowest singlet excited state, a broad structureless excited-state absorption (ESA) band appears instantaneously peaking at ~470 nm. This band has been previously assigned to a S_1-S_n transition in the TIPS-PN molecule [46, 47]. A second ESA band appears in the near-infrared region at ~1400 nm. The negative ΔA signal near ~680 nm is primarily assigned to ground-state bleach, consistent with the ground-state absorption maximum of TIPS-PhPN. Stimulated emission is expected to contribute mainly on the red side of this negative feature, where it overlaps with the steady-state fluorescence band. Figure 3a,b show the TA maps, and Figure 3c,d show the representative time-resolved spectra at of TIPS-PhPN in the visible and near-infrared probe ranges, respectively. The transient spectral features of TIPS-PhPN are similar to that of TIPS-PN (Figure S30) albeit a shift in the peak wavelength of the ESA bands, but the lack of vibronic structure associated with the ESA band is prominent in the former. A comparison of kinetic traces at the ESA in the 450 nm region (Figure 3e) and the peak position of the GSB-dominated negative signal (Figure 3f) among the TIPS-PhPN, TIPS-PN and TIPS-isoPhPN show that the singlet state in TIPS-PhPN loses population on a relatively faster timescale than TIPS-PN and TIPS-isoPhPN.

To understand the excited-state dynamics during the earlier timescale after photoexcitation, global analysis of the transient data was performed in GLOTARAN using a sequential kinetic model to the data measured in the visible probe window (420–770 nm) and the near-infrared window (850–1500 nm) [48, 49]. Representative kinetic traces together with the corresponding global fits and residuals are provided in Figure S31 to demonstrate the adequacy of the kinetic model. The residuals show no systematic spectral or temporal structure within the signal-to-noise level of the measurements. Global analysis predicted three components: 1–2 ps, 20–30 ps and a nanoseconds-long time-component by modeling the data measured in the 7 ns time-window in our femtosecond TA setup. The corresponding evolution-associated spectra (EAS)—which predict spectral signatures of populations evolving with these kinetic components—show differences in the peak positions and bandwidths of the ESA bands for the first and second time-components compared to the nanosecond-scale third time-component (Figure 4a,b). The spectral differences in the ESA band at ~470 nm are modest (Figure 4a) in comparison to the more pronounced spectral changes in the near-infrared band at ~1400 nm (Figure 4b). In the latter case, the 1–2 ps EAS exhibits a narrow bandwidth peaking near 1425 nm, and the 20–30 ps EAS displays a larger bandwidth with the peak shifted to ~1400 nm (Figure 4b). The early-time spectral evolution also necessitate the inclusion of an additional 100–200 fs time component in the near-infrared data, with an EAS peaking at ~1440 nm, resulting in improved fitting close to time zero (Figure 4b). When compared across the three pentacene analogs, the spectral shift and broadening observed in the near-infrared ESA band in TIPS-PhPN (Figure 4c) are more pronounced than TIPS-PN (Figure 4d) and TIPS-isoPhPN (Figure 4e). Additionally, the second time-component converges to a lower value of ~10 ps in TIPS-PN and TIPS-isoPhPN compared to ~30 ps in TIPS-PhPN. This is consistent with the observation that the spectral shifts in TIPS-PN are less prominent than those in TIPS-PhPN.

2.3.2 | Spectral Assignment of the Picosecond-Long Time-Components

The femto- to picosecond-long time-components in TIPS-PN have previously been assigned to vibrational and solvent relaxations in the singlet excited state [50, 51]. TIPS-PhPN, as noted above, exhibits several distinct features. In the visible region, the short-lived negative DAS contribution near ~680 nm reflects early-time spectral relaxation and reshaping within the GSB-dominated negative band, with possible stimulated-emission contribution on the red side, rather than the decay of a distinct transient species. Most notably, the ESA feature in the near-infrared region around 1400 nm undergoes pronounced broadening that is unique to TIPS-PhPN (Figure 4c). Close to time zero, the ESA band is relatively narrow, peaking at ~1440 nm. The EAS associated with the 100–200 fs time component displays two maxima, at 1440 nm and ~900 nm, and shows reduced absorption at the vibronic feature near 1200 nm. The decay associated spectra (DAS) from global analysis corresponding to this component predicts a loss of population (positive feature) at 1440 nm, switching to a negative feature (population growth) at shorter wavelengths on this timescale. This growth does not reflect the formation of a new electronic state but rather the spectral shift of the ESA band, which peaks at ~1425 nm in the EAS for the 1–2 ps component. This peak shift is accompanied by a loss of intensity and broadening of the ESA toward shorter wavelengths. The shifting and broadening continue in the third EAS with a time constant of 30–40 ps.

The shifting and broadening of the 1400 nm ESA band can be attributed to the sensitivity of the electronic-state energy to the torsional flexibility in TIPS-PhPN. A shift of the transition energy to shorter wavelengths reflects an increase in the S_1–S_n energy gap, arising from stabilization of the lower excited state as the molecule relaxes along the torsional coordinate. Because this effect is not observed to a similar extent in TIPS-PN or TIPS-isoPhPN, solvent reorganization can largely be excluded, and torsional stabilization emerges as the dominant factor. Furthermore, a narrowband photoexcitation initially promotes a sub-ensemble of ground-state geometries into the Franck–Condon state, consistent with spectral hole burning [52, 53]. This explains the narrow ESA band observed immediately after

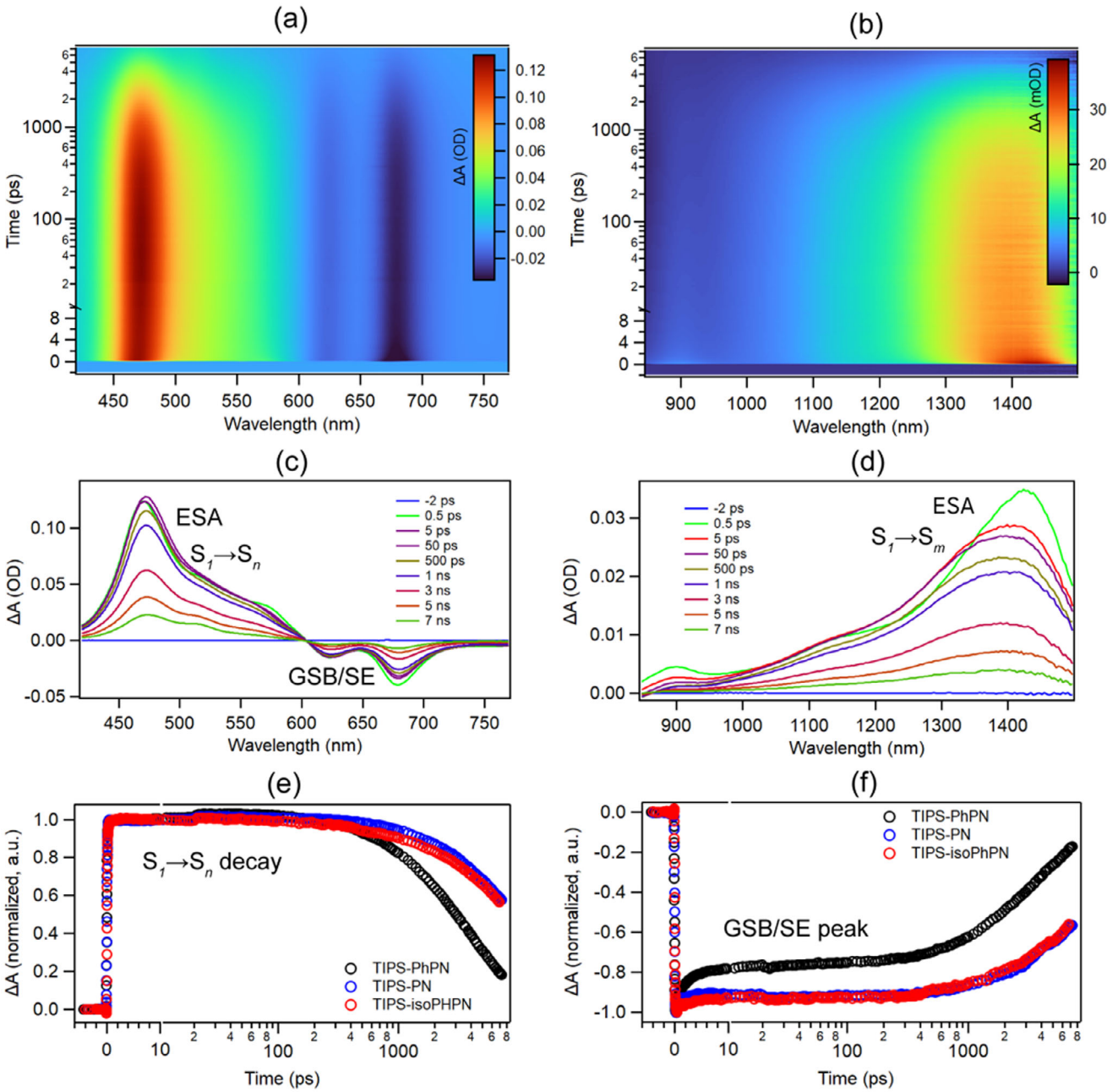

FIGURE 3 | Femtosecond transient absorption maps of air-equilibrated TIPS-PhPN (0.32 mM) in tetrahydrofuran solvent in the visible (a) and near-infrared (b) probe spectral regions, with representative time-resolved spectra at various delay times after photoexcitation shown in (c) and (d). The time axis is split between linear from -2 to 10 ps and logarithmic from 10 ps–7 ns. Representative kinetic traces extracted at the excited-state absorption spectral region (e) and peak ground-state bleach/stimulated emission signal (f) for TIPS-PhPN, TIPS-PN and TIPS-isoPhPN are shown.

excitation, as captured in the EAS associated with the 100–200 fs component. With time, this initially selective population redistributes across a broader set of configurations, producing a wider distribution of excited states geometries and leading to the broadening of the ESA near 1400 nm. This observation strongly supports the above theoretical prediction that the torsional PES in TIPS-PhPN is extremely shallow in both ground and excited states and accommodates a broader range of configurations with torsional angles ranging from 0° to 60° (Figure 2 and Figure S22). The broader vibronic features in the steady-state absorption spectrum of TIPS-PhPN, compared with the other two analogs, further support this picture. One possible reason that the near-infrared ESA is more sensitive to torsional flexibility than the 470 nm ESA is the stronger dependence of the higher-lying electronic state (S_n) on phenyl-ring configurations. The 1400 nm ESA band progressively broadens and reaches its fully developed spectral width within tens of picoseconds, consistent with torsional relaxation timescales reported for other molecular systems [54, 55]. To further establish the role of torsional motions, transient absorption dynamics was measured in a polystyrene (PS) matrix, which effectively suppresses large-amplitude motions. In this rigid environment, no time-dependent changes in spectral position or bandwidth of the 1400 nm ESA band were observed, and the ESA bandwidth remains consistently narrow at all

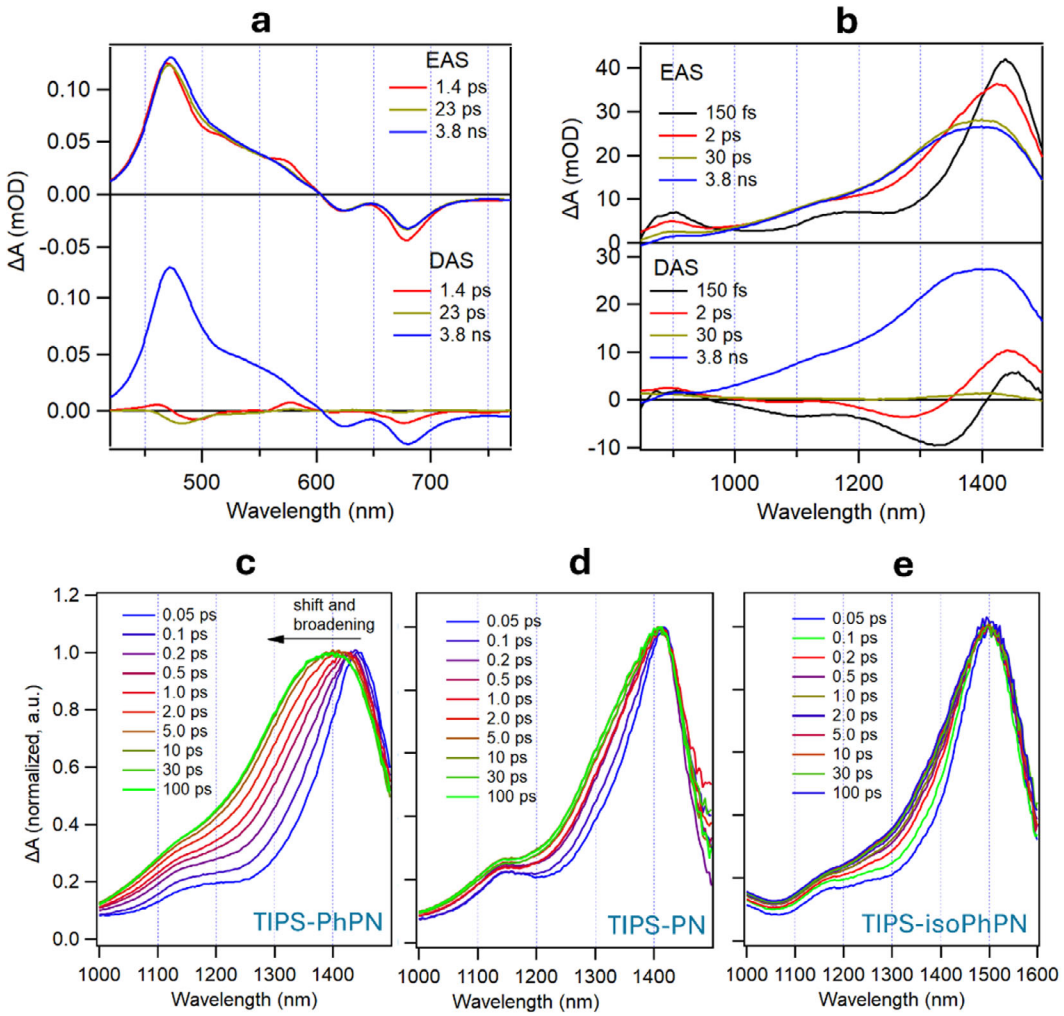

FIGURE 4 | The evolution associated spectra (EAS) and decay associated spectra (DAS) of various time-components predicted by the global analysis of TIPS-PhPN data in the visible and near-infrared spectral regions are shown in (a) and (b). Plots (c–e) shows the transient absorption spectra at representative waiting-times from 50 fs to 100 ps in the near-infrared probing region normalized to the maximum absorbance of the ESA band at ~1400 nm for TIPS-PhPN, TIPS-PN, and TIPS-isoPhPN.

waiting times, confirming that torsional flexibility underlies the early-time excited-state dynamics in TIPS-PhPN.

2.3.3 | Nano- to Microsecond Dynamics

At waiting times longer than 100 ps up until 7 ns, all transient spectral features decay consistently without a noticeable shift or change in bandwidth. This decay represents the lifetime of the photoexcited singlet state (Figure 5a,b). Toward the end of the ~7 ns time-window of our femtosecond TA setup, a new peak begins to emerge near ~515 nm underneath the singlet ESA signal in TIPS-PhPN, and a similar excited-state dynamics follows in TIPS-PN and TIPS-isoPhPN. The long-time excited state dynamics in these analogs was tracked using a nanosecond transient absorption setup offering a time-window extending from nanoseconds to microseconds with a ~500 ps time-resolution (Figure 5a).

Global analysis of the nanosecond TA data of TIPS-PhPN reveals a prominent singlet lifetime component of 3.8 ns in THF. Analysis of the photophysical rate constants shows that nonradiative decay strongly dominates over radiative relaxation, with a nonradiative rate constant of 2.4×10^8 s^{-1} compared to a radiative rate constant of 2.0×10^7 s^{-1}. This imbalance is consistent with the low fluorescence quantum yield observed for TIPS-PhPN. We propose that this enhanced nonradiative decay arises from large-amplitude torsional flexibility in the excited state which stabilizes the excited singlet state and reduces the ground-excited energy gap. As per the energy gap law, such stabilization increases vibronic coupling between electronic and vibrational manifolds, thereby accelerating internal conversion [56]. Torsional motion is well known to introduce efficient nonradiative pathways by enabling access to lower-energy conformations [57]. On the contrary, TIPS-PN and TIPS-isoPhPN lack a dominant torsion-driven lowering of singlet energy and thus boast longer singlet lifetime of 11 ns and 10.4 ns respectively (Figure 5b), and a correspondingly high fluorescence quantum yield. To further confirm the role of torsional motion, as shown in Figure 5b, the S_1 lifetime of TIPS-PhPN doubles from 3.8 ns in THF solution to 8 ns in the polystyrene matrix (210% increase), whereas the corresponding increase in lifetime is modest for TIPS-PN (11 → 15 ns, 136%) and TIPS-isoPhPN (10.4 → 16 ns, 154%).Temperature-dependent

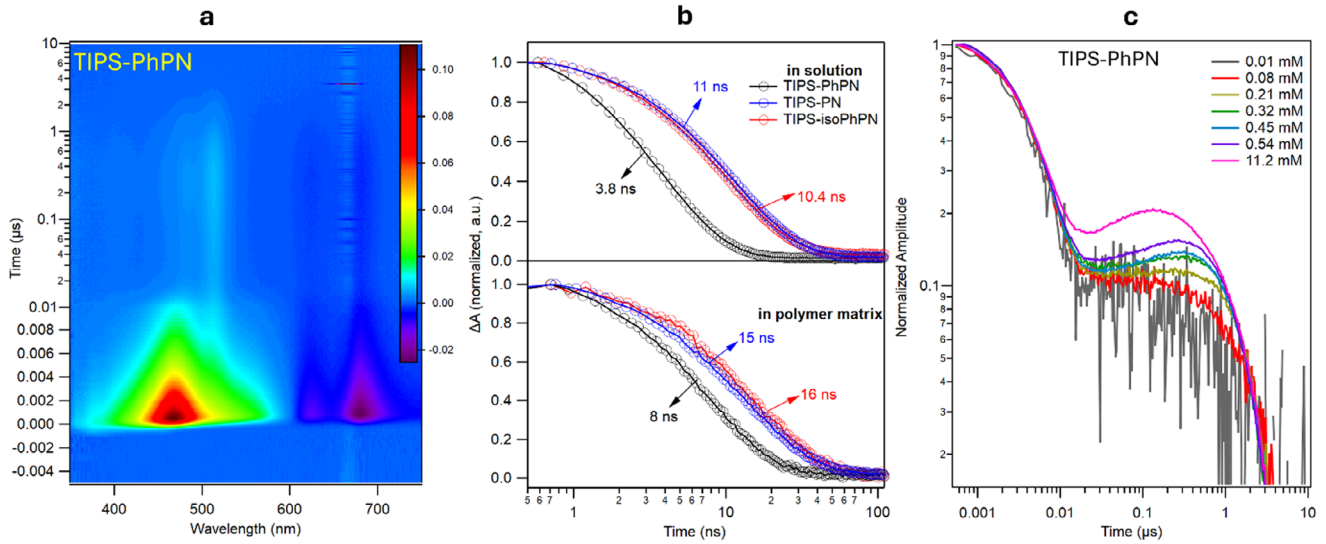

FIGURE 5 | A nanosecond-microsecond transient absorption map of air-equilibrated TIPS-PhPN (0.54 mM) solution in THF solvent is shown in (a) with −5 to 10 ns plotted as a linear range and 10 ns to 10 μs as a logarithmic range along the vertical axis, emphasizing on the singlet absorption signal in the nanosecond timescale and triplet absorption signal in the nano-microsecond timescale. (b), kinetics traces of TIPS-PhPN, TIPS-PN and TIPS-isoPhPN extracted at the peak ESA signal in the visible region, in the solution phase (above) and polymer phase (below). The kinetic traces are normalized at the maximum. (c), Kinetic traces extracted at 520 nm, where triplet absorption signal peaks, are plotted for different concentrations of TIPS-PhPN in THF solution. The y-axis is plotted as a logarithmic scale to emphasize the varying timescale corresponding to the growth of the triplet signal.

lifetime measurements would provide an additional test of the role of torsional motion in the excited-state decay. However, changing temperature in solution would also alter solvent viscosity, diffusion, intermolecular encounter rates, and potentially the efficiency of diffusion-limited singlet fission. The PS matrix measurements were therefore included as a fixed-temperature control to restrict large-amplitude structural relaxation, including torsional motion, without simultaneously changing these solution-phase variables. The larger relative increase in the S1 lifetime of TIPS-PhPN in PS compared with TIPS-PN and TIPS-isoPhPN is therefore consistent with a stronger contribution of torsional relaxation to the nonradiative decay of TIPS-PhPN.

The decay of the singlet spectral signals is followed by the growth of a new spectral feature peaking at ~515 nm in TIPS-PhPN (Figure 5a). In the case of TIPS-PN in solution, this spectral signal, peaked at ~500 nm, has been well-established and assigned to a triplet-triplet ($T_1 - T_n$) absorption signal [47, 58, 59]. In TIPS-isoPhPN, the same spectral signal appears at ~520 nm. For TIPS-PhPN, we performed a series of concentration-dependent measurements in the nano-microsecond range, where the concentrations of TIPS-PhPN were set at 0.01, 0.08, 0.21, 0.32, 0.45, 0.54, and 11.2 mM (Figure 5c). All measurements were performed in a cuvette of 1 mm pathlength except the 11.2 mM concentration which was measured in a 0.2 mm pathlength cuvette. We observe that this triplet feature grows gradually ranging from tens of nanoseconds in high-concentration solutions to hundreds of nanoseconds in low-concentration solutions. Notably, the growth timescale is much longer than the decay of the singlet state (3.8 ns), as was the case in TIPS-PN. Such delayed growth has previously been attributed to diffusion-mediated molecular encounters, in which randomly colliding pentacene molecules form correlated triplet pairs within the singlet-state lifetime [47]. These correlated pairs subsequently dissociate into individual triplets, giving rise to the observed growth of the triplet signal. The triplet states then decay back to the ground state on a few-microsecond timescale. The delayed peaking of the triplet absorption signal and its concentration dependence confirms that these triplets are not formed directly through intersystem crossing, but an outcome of diffusion-limited singlet fission. Although these observations indicate that diffusion-limited singlet fission is the dominant source of triplet population in solution, we cannot completely rule out a minor contribution from intersystem crossing. A weak triplet signal is still observed at the lowest concentration measured, 10 μM, and a small triplet-like absorption is also observed in the polystyrene matrix, where diffusion-mediated encounters are strongly suppressed. However, because the solution-phase triplet population is dominated by singlet-fission-generated triplets, an absolute triplet quantum yield measured under these conditions would represent an apparent, concentration-, fluence-, and environment-dependent total triplet yield rather than an intrinsic ISC yield. Therefore, while minor ISC may contribute to the residual triplet signal, the delayed growth kinetics and concentration dependence support diffusion-limited singlet fission as the primary triplet formation pathway, with internal conversion serving as the dominant nonradiative decay pathway of the singlet state.

These results provide direct evidence to the computational results that torsional motion is the main coordinate that promotes internal conversion in TIPS-PhPN. The spectral broadening and shifting of the 1400 nm ESA band, combined with the suppression of nonradiative pathways in the PS matrix, highlight the strong coupling between torsional degrees of freedom and electronic relaxation. Importantly, the magnitude of the torsional effect being much larger in TIPS-PhPN than in the other analogs,

underscores that substitution at the phenyl position enhances torsional flexibility and thereby accelerates nonradiative decay. In summary, torsional flexibility not only explains the unique spectral dynamics of TIPS-PhPN but also rationalizes its markedly shorter excited-state lifetime compared to TIPS-PN and TIPS-isoPhPN.

2.4 | Photostability

A highly beneficial outcome of the unique optical properties of the newly developed pentacene materials is their increased photostability over TIPS-PN. In the presence of molecular oxygen, the excited states of acenes can generate reactive oxygen species (ROS); either singlet oxygen by energy transfer from triplet states, or other ROS such as superoxide by electron transfer from singlet states. The photo-generated ROS can then react with ground-state acene molecules by [4+2] cycloaddition across one of the more central benzenoid rings [60]. TIPS-PN has already been shown to possess surprisingly good photostability compared to shorter acenes [61], as the T_1 energy drops below that of the triplet-to-singlet excitation of oxygen, meaning that the energy transfer pathway to material decomposition becomes unavailable [62]. TIPS-PhPN and TIPS-isoPhPN are predicted to have similar T_1 energies so should also benefit from increased photostability.

The ambient photostability of the three materials was compared in three different solvents under otherwise identical conditions, using a 90W halogen lamp (Figure S34) directed onto the sample cuvette via fiber optic cable. The absorption at 590 nm was continuously monitored over 15 min of illumination, and the linear fit of decrease in absorbance used as a measure of initial rate for the photo-oxidation reaction.

TIPS-PhPN showed almost no photo-oxidation under illumination in chloroform compared to the other two pentacenes (Figure 6). Comparing the slopes of the initial loss in absorption, TIPS-PhPN reacts significantly more slowly (k_{rel} = 0.16) than TIPS-PN and TIPS-isoPhPN, with all three pentacenes absorbing the same amount of the white light (estimated by integration of the overlap of white light and PN absorption spectra, Figure S34). Photostability is solvent-dependent due to solvent quenching of excited states and the concentration of molecular oxygen in air-equilibrated solvent [62]. Side-by-side experiments in aerated versus degassed solvent (Figures S35–37) show that any decomposition is due to endoperoxide formation rather than photo-dimerization, where the oxidation is predominantly from electron transfer of singlet states since the triplet energies are too low for singlet oxygen sensitization [60–62]. We have previously shown that an important factor of acene photostability is the relative stabilization of both the acene and endoperoxide products by various substituents [63]. Therefore the reaction between ROS and ground state pentacene was modeled by DFT calculations (Figure S38), and showed that TIPS-PhPN should be slightly more reactive than TIPS-PN. Therefore, the increased photostability must arise from smaller amounts of ROS being produced, stemming from the fact that the excited states have shorter lifetimes (e.g. through radiationless relaxation via rotational modes of phenyl rings and core torsion). This is also evident from the quantum yield measurements with degassed

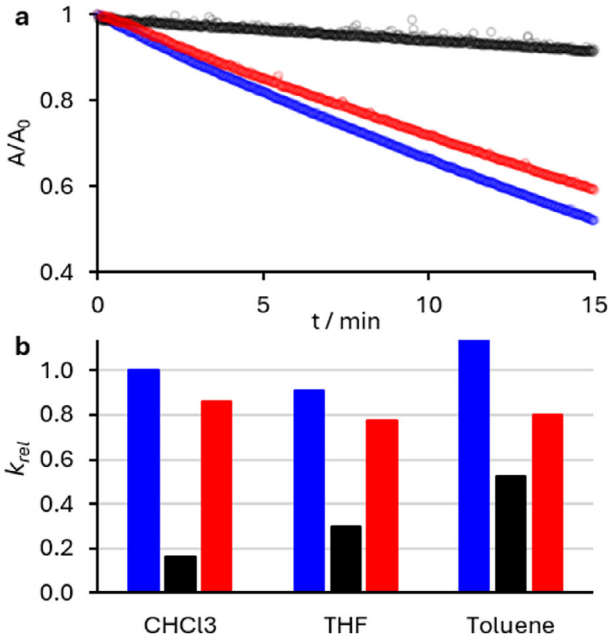

FIGURE 6 | Photostability comparison between TIPS-PN, TIPS-PhPN, and TIPS-isoPhPN measured at equal concentration (5×10^{-5} M at 298 K) under illumination by white light. (a) Absorbance at 590 nm over time during light irradiation, normalized at t = 0. (b) Relative rate of photo-oxidation of pentacenes in different solvents (versus TIPS-PN in $CHCl_3$).

solvent, where TIPS-PhPN excited states were not quenched by the presence of oxygen. TIPS-isoPhPN shows a modest increase in photostability versus TIPS-PN, indicating that while electron-donating effects of the phenyl groups have some influence, the majority of the stabilization toward photo-oxidation should come from the torsion of the pentacene core via deactivation of the excited states.

3 | Conclusions

We have investigated the optical properties of two silylethynyl pentacenes bearing additional phenyl substituents on the acene core. The previously reported TIPS-PhPN possesses a twisted pentacene core, where density functional theory (DFT) calculations reveal a shallow potential energy surface for contortion. The newly synthesized isomer bearing phenyl groups on the end rings of the pentacene does not show the twisted pentacene motif, but still has red-shifted absorption compared to parent TIPS-PN. Through a combination of structural variation in DFT calculations and comparison of steady state optical spectra of these three materials, the source of broadened red-shifted absorption in TIPS-PhPN was assigned less to the pentacene core twisting itself, but from resonance effects of the phenyl rings which become partially planarized during this twist. TIPS-PhPN exhibits much weaker emission than the other materials, with the difference being the shallow energy surfaces of the distorted pentacene system. Ultra-fast transient spectroscopy reveals broadened excited state absorption in TIPS-PhPN, which shifts over time as the molecular geometry evolves along the pentacene torsional motion. TIPS-PhPN exhibits short excited state lifetimes which are dramatically affected by suppression of geometry

changes by a polymer matrix when compared to the other two pentacenes. The result of these unique optical properties is that TIPS-PhPN exhibits much more resilience to photo-oxidation, making for a more stable material than TIPS-PN stemming from the shallow torsional PES and non-radiative deactivation of the excited states. This increase in molecular stability does not come at the cost of functionality, as TIPS-PhPN has already shown sizeable charge mobility in transistor devices [29], while their potential as singlet fission materials is currently under further investigation.

Acknowledgements

The authors thank the National Science Foundation (DMR-2414541) for support of the synthesis of pentacene derivatives and the U.S. Department of Energy (DOE EPSCoR, DE-SC0025355) for support of the spectroscopic and computational characterization. A.S. and S.R.R. acknowledge the financial support through startup fund from the University of Kentucky.

Funding

This work is supported by the National Science Foundation (DMR-2414541) for support of the Synthesis of Pentacene Derivatives. U.S. Department of Energy (DOE EPSCoR, DE-SC0025355) for support of the spectroscopic and computational Characterization.

Conflicts of Interest

The authors declare no conflicts of interest.

Data Availability Statement

The data that support the findings of this study are available from the corresponding author upon reasonable request. CCDC 2542392 contains the supplementary crystallographic data for this paper. These data can be obtained free of charge from The Cambridge Crystallographic Data Centre via www.ccdc.cam.ac.uk/data_request/cif.

References

1. V. Brega, Y. Yan, and S. W. Thomas, "Acenes beyond Organic Electronics: Sensing of Singlet Oxygen and Stimuli-Responsive Materials," *Organic & Biomolecular Chemistry* 18, no. 45 (2020): 9191–9209, https://doi.org/10.1039/D0OB01744B.

2. K. Kuroda, K. Yazaki, Y. Tanaka, et al., "A Pentacene-Based Nanotube Displaying Enriched Electrochemical and Photochemical Activities," *Angewandte Chemie International Edition* 58, no. 4 (2019): 1115–1119, https://doi.org/10.1002/anie.201812976.

3. A.-S. Wollny, G. Lavarda, I. Papadopoulos, et al., "Förster Resonance Energy Transfer Sensitized Singlet Fission in BODIPY-Pentacene Dimer Conjugates," *Advanced Optical Materials* 11, no. 19 (2023): 2300500, https://doi.org/10.1002/adom.202300500.

4. Y. Gan, S. Qin, Q. Du, et al., "Ultrafast and Sensitive Self-Powered Photodetector Based on Graphene/Pentacene Single Crystal Heterostructure with Weak Light Detection Capacity," *Advanced Science* 9, no. 35 (2022): 2204332, https://doi.org/10.1002/advs.202204332.

5. S. Wei, H. W. Choi, G. Jabbour, A. Nathan, and J. Yu, "Fully Inkjet-Printed, Flexible TIPS-Pentacene Photodetector for Photoplethysmogram," *Advanced Optical Materials* 13, no. 31 (2025): 01942, https://doi.org/10.1002/adom.202501942.

6. Y.-F. Lim, Y. Shu, S. R. Parkin, J. E. Anthony, and G. G. Malliaras, "Soluble n-Type Pentacene Derivatives as Novel Acceptors for Organic Solar Cells," *Journal of Materials Chemistry* 19, no. 19 (2009): 3049–3056, https://doi.org/10.1039/B818693F.

7. J. E. Anthony, "Functionalized Acenes and Heteroacenes for Organic Electronics," *Chemical Reviews* 106, no. 12 (2006): 5028–5048, https://doi.org/10.1021/cr050966z.

8. B. Purushothaman, M. Bruzek, S. R. Parkin, A.-F. Miller, and J. E. Anthony, "Synthesis and Structural Characterization of Crystalline Nonacenes," *Angewandte Chemie International Edition* 50, no. 31 (2011): 7013–7017, https://doi.org/10.1002/anie.201102671.

9. A. D. Platt, J. Day, S. Subramanian, J. E. Anthony, and O. Ostroverkhova, "Optical, Fluorescent, and (Photo)Conductive Properties of High-Performance Functionalized Pentacene and Anthradithiophene Derivatives," *The Journal of Physical Chemistry C* 113, no. 31 (2009): 14006–14014, https://doi.org/10.1021/jp904021p.

10. B. M. Medina, J. E. Anthony, and J. Gierschner, "Independent Tuning of Electronic Levels in Pentacene by Site-Specific Substitution," *Chemphyschem* 9, no. 11 (2008): 1519–1523, https://doi.org/10.1002/cphc.200800122.

11. M. B. Smith and J. Michl, "Singlet Fission," *Chemical Reviews* 110, no. 11 (2010): 6891–6936, https://doi.org/10.1021/cr1002613.

12. K. Broch, J. Dieterle, F. Branchi, et al., "Robust Singlet Fission in Pentacene Thin Films with Tuned Charge Transfer Interactions," *Nature Communications* 9, no. 1 (2018): 954, https://doi.org/10.1038/s41467-018-03300-1.

13. S. M. Hart, W. R. Silva, and R. R. Frontiera, "Femtosecond Stimulated Raman Evidence for Charge-Transfer Character in Pentacene Singlet Fission," *Chemical Science* 9, no. 5 (2018): 1242–1250, https://doi.org/10.1039/C7SC03496B.

14. G. Lavarda, A. Sharma, M. Beslać, et al., "Long-Lived Triplets from Singlet Fission in Pentacene-Decorated Helical Supramolecular Polymers," *Journal of the American Chemical Society* 146, no. 42 (2024): 28985–28993, https://doi.org/10.1021/jacs.4c09844.

15. H. Seiler, M. Krynski, D. Zahn, et al., "Nuclear Dynamics of Singlet Exciton Fission in Pentacene Single Crystals," *Science Advances* 7, no. 26 (2021): abg0869, https://doi.org/10.1126/sciadv.abg0869.

16. J. Zirzlmeier, D. Lehnherr, P. B. Coto, et al., "Singlet Fission in Pentacene Dimers," *Proceedings of the National Academy of Sciences* 112, no. 17 (2015): 5325–5330, https://doi.org/10.1073/pnas.1422436112.

17. F. Plasser, H. Pašalić, M. H. Gerzabek, et al., "The Multiradical Character of One- and Two-Dimensional Graphene Nanoribbons," *Angewandte Chemie International Edition* 52, no. 9 (2013): 2581–2584, https://doi.org/10.1002/anie.201207671.

18. N. A. Pace, T. T. Clikeman, S. H. Strauss, et al., "Triplet Excitons in Pentacene Are Intrinsically Difficult to Dissociate via Charge Transfer," *The Journal of Physical Chemistry C* 124, no. 48 (2020): 26153–26164, https://doi.org/10.1021/acs.jpcc.0c08537.

19. N. V. Korovina, J. Joy, X. Feng, et al., "Linker-Dependent Singlet Fission in Tetracene Dimers," *Journal of the American Chemical Society* 140, no. 32 (2018): 10179–10190, https://doi.org/10.1021/jacs.8b04401.

20. V. Abraham and N. J. Mayhall, "Simple Rule To Predict Boundedness of Multiexciton States in Covalently Linked Singlet-Fission Dimers," *The Journal of Physical Chemistry Letters* 8, no. 22 (2017): 5472–5478, https://doi.org/10.1021/acs.jpclett.7b02476.

21. P. M. Zimmerman, F. Bell, D. Casanova, and M. Head-Gordon, "Mechanism for Singlet Fission in Pentacene and Tetracene: from Single Exciton to Two Triplets," *Journal of the American Chemical Society* 133, no. 49 (2011): 19944–19952, https://doi.org/10.1021/ja208431r.

22. M. H. Futscher, A. Rao, and B. Ehrler, "The Potential of Singlet Fission Photon Multipliers as an Alternative to Silicon-Based Tandem Solar Cells," *ACS Energy Letters* 3, no. 10 (2018): 2587–2592, https://doi.org/10.1021/acsenergylett.8b01322.

23. A. J. Baldacchino, M. W. Brett, B. P. Carwithen, et al., "Singlet Fission c-Si Solar Cells: Beyond Tetracene," *ACS Energy Letters* 10, no. 9 (2025): 4596–4602, https://doi.org/10.1021/acsenergylett.5c01930.

24. A. J. Baldacchino, M. I. Collins, M. P. Nielsen, T. W. Schmidt, D. R. McCamey, and M. J. Y. Tayebjee, "Singlet Fission Photovoltaics: Progress and Promising Pathways," *Chemical Physics Reviews* 3, no. 2 (2022): 021304, https://doi.org/10.1063/5.0080250.

25. M. A. Baldo, N. J. Ekins-Daukes, J. Y. Jiang, P. M. Pearce, T. W. Schmidt, and M. J. Y. Tayebjee, "Singlet Fission Provides a Scalable Pathway to High Efficiency Silicon Photovoltaics," *ACS Energy Letters* 10, no. 10 (2025): 4830–4833, https://doi.org/10.1021/acsenergylett.5c01944.

26. B. K. Rugg, K. E. Smyser, B. Fluegel, et al., "Triplet-Pair Spin Signatures from Macroscopically Aligned Heteroacenes in an Oriented Single Crystal," *Proceedings of the National Academy of Sciences* 119, no. 29 (2022): 2201879119.

27. K. E. Smyser and J. D. Eaves, "Singlet Fission for Quantum Information and Quantum Computing: The Parallel JDE Model," *Scientific Reports* 10, no. 1 (2020): 18480, https://doi.org/10.1038/s41598-020-75459-x.

28. A. Yamauchi, K. Tanaka, M. Fuki, et al., "Room-temperature Quantum Coherence of Entangled Multiexcitons in a Metal-organic Framework," *Science Advances* 10 (2024): adi3147, https://doi.org/10.1126/sciadv.adi3147.

29. K. J. Thorley, G. S. Rupasinghe, S. Ruhunage, et al., "Simple Synthesis, Structural and Electronic Characterization of Soluble Contorted Pentacenes," *Chemistry of Materials* 38, no. 7 (2026): 3704–3714, https://doi.org/10.1021/acs.chemmater.6c00263.

30. J. Zhang, S. Sarrafpour, T. E. Haas, P. Müller, and S. W. Thomas, "Structure, Photophysics, and Photooxidation of Crowded Diethynyltetracenes," *Journal of Materials Chemistry* 22, no. 13 (2012): 6182–6189, https://doi.org/10.1039/C2JM16173G.

31. A. S. Paraskar, A. R. Reddy, A. Patra, et al., "Rubrenes: Planar and Twisted," *Chemistry – A European Journal* 14 (2008): 10639–10647, https://doi.org/10.1002/chem.200800802.

32. P. Ludwig, F. Rominger, J. Freudenberg, and U. H. F. Bunz, "Stabilization of Acenes: "Geländer"-Pentacenes," *Angewandte Chemie International Edition* 63, no. 13 (2024): 202316902, https://doi.org/10.1002/anie.202316902.

33. P. Malakar, V. Borin, A. Bedi, I. Schapiro, O. Gidron, and S. Ruhman, "The Impact of Twisting on the Intersystem Crossing in acenes: an Experimental and Computational Study," *Physical Chemistry Chemical Physics* 24, no. 4 (2022): 2357–2362, https://doi.org/10.1039/D1CP05728F.

34. M. M. Safont-Sempere, P. Osswald, M. Stolte, et al., "Impact of Molecular Flexibility on Binding Strength and Self-Sorting of Chiral π-Surfaces," *Journal of the American Chemical Society* 133, no. 24 (2011): 9580–9591, https://doi.org/10.1021/ja202696d.

35. M. Gsänger, J. H. Oh, M. Könemann, et al., "A Crystal-Engineered Hydrogen-Bonded Octachloroperylene Diimide with a Twisted Core: an n-Channel Organic Semiconductor," *Angewandte Chemie International Edition* 49, no. 4 (2010): 740–743, https://doi.org/10.1002/anie.200904215.

36. Y. Dong, Z. Zhang, Y. Hashikawa, H. Meng, F. Bai, and K. Itami, "A Double Twisted Nanographene with a Contorted Pyrene Core," *Angewandte Chemie International Edition* 63 (2024): 202406927, https://doi.org/10.1002/anie.202406927.

37. K. M. Magiera, V. Aryal, and W. A. Chalifoux, "Alkyne Benzannulations in the Preparation of Contorted Nanographenes," *Organic & Biomolecular Chemistry* 18, no. 13 (2020): 2372–2386, https://doi.org/10.1039/D0OB00182A.

38. X. Yang, F. Rominger, and M. Mastalerz, "Contorted Polycyclic Aromatic Hydrocarbons with Two Embedded Azulene Units," *Angewandte Chemie International Edition* 58, no. 49 (2019): 17577–17582, https://doi.org/10.1002/anie.201908643.

39. A. Swain, F. Rominger, and M. Mastalerz, "C2-Symmetric Perylene-Embedded Double [5]Helicenes," *Organic Letters* 27, no. 31 (2025): 8770–8775, https://doi.org/10.1021/acs.orglett.5c02745.

40. T. Kawashima, Y. Matsumoto, T. Sato, et al., "Synthesis, Structure, and Complexation of an S-Shaped Double Azahelicene with Inner-Edge Nitrogen Atoms," *Chemistry – A European Journal* 26 (2020): 13170–13176, https://doi-org.ezproxy.uky.edu/10.1002/chem.202002405.

41. Q. Jiang, Y. Han, Y. Zou, et al., "S-shaped Para-Quinodimethane-Embedded Double [6]Helicene and Its Charged Species Showing Open-Shell Diradical Character," *Chemistry – A European Journal* 26 (2020): 15613–15622, https://doi.org/10.1002/chem.202002952.

42. Y. Shen and C.-F. Chen, "Helicenes: Synthesis and Applications," *Chemical Reviews* 112, no. 3 (2012): 1463–1535, https://doi.org/10.1021/cr200087r.

43. N. Han, C. Hou, Z. Duan, J. Gu, Y. Zhang, and J. Luo, "9-Diaryl-6,13-bis(triisopropylsilylethynyl)Pentacene Derivatives: Synthesis and Application in Cancer Sonodynamic Therapy," *Chemical Communications* 61 (2025): 5174–5177, https://doi.org/10.1039/D5CC00326A.

44. J. E. Norton and K. N. Houk, "Electronic Structures and Properties of Twisted Polyacenes," *Journal of the American Chemical Society* 127, no. 12 (2005): 4162–4163, https://doi.org/10.1021/ja042379l.

45. A. Bedi and O. Gidron, "The Consequences of Twisting Nanocarbons: Lessons from Tethered Twisted Acenes," *Accounts of Chemical Research* 52, no. 9 (2019): 2482–2490, https://doi.org/10.1021/acs.accounts.9b00271.

46. C. Ramanan, A. L. Smeigh, J. E. Anthony, T. J. Marks, and M. R. Wasielewski, "Competition between Singlet Fission and Charge Separation in Solution-Processed Blend Films of 6,13-Bis(triisopropylsilylethynyl)Pentacene with Sterically-Encumbered Perylene-3,4:9,10-bis(dicarboximide)s," *Journal of the American Chemical Society* 134, no. 1 (2012): 386–397, https://doi.org/10.1021/ja2080482.

47. B. J. Walker, A. J. Musser, D. Beljonne, and R. H. Friend, "Singlet Exciton Fission in Solution," *Nature Chemistry* 5, no. 12 (2013): 1019–1024, https://doi.org/10.1038/nchem.1801.

48. S. R. Rather, M. J. Bezdek, M. Koch, P. J. Chirik, and G. D. Scholes, "Ultrafast Photophysics of a Dinitrogen-Bridged Molybdenum Complex," *Journal of the American Chemical Society* 140, no. 20 (2018): 6298–6307, https://doi.org/10.1021/jacs.8b00890.

49. J. J. Snellenburg, S. Laptenok, R. Seger, K. M. Mullen, and I. H. M. van Stokkum, "Glotaran: A Java-Based Graphical User Interface for the R Package TIMP," *Journal of Statistical Software* 49, no. 3 (2012): 1–22, 10.18637/jss.v049.i03.

50. N. Alagna, J. L. Pérez Lustres, N. Wollscheid, et al., "Singlet Fission in Tetraaza-TIPS-Pentacene Oligomers: From Fs Excitation to Ms Triplet Decay via the Biexcitonic State," *The Journal of Physical Chemistry B* 123, no. 50 (2019): 10780–10793, https://doi.org/10.1021/acs.jpcb.9b08031.

51. C. Grieco, G. S. Doucette, R. D. Pensack, et al., "Dynamic Exchange during Triplet Transport in Nanocrystalline TIPS-Pentacene Films," *Journal of the American Chemical Society* 138, no. 49 (2016): 16069–16080, https://doi.org/10.1021/jacs.6b10010.

52. F. R. Kohl, C. Grieco, and B. Kohler, "Ultrafast Spectral Hole Burning Reveals the Distinct Chromophores in Eumelanin and Their Common Photoresponse," *Chemical Science* 11, no. 5 (2020): 1248–1259, https://doi.org/10.1039/C9SC04527A.

53. T. A. A. Oliver, "Recent Advances in Multidimensional Ultrafast Spectroscopy," *Royal Society Open Science* 5, no. 1 (2018): 171425, https://doi.org/10.1098/rsos.171425.

54. J. Clark, T. Nelson, S. Tretiak, G. Cirmi, and G. Lanzani, "Femtosecond Torsional Relaxation," *Nature Physics* 8, no. 3 (2012): 225–231, https://doi.org/10.1038/nphys2210.

55. G. Li, D. Magana, and R. B. Dyer, "Direct Observation and Control of Ultrafast Photoinduced Twisted Intramolecular Charge Transfer (TICT) in Triphenyl-Methane Dyes," *The Journal of Physical Chemistry B* 116 (2012): 12590–12596, https://doi.org/10.1021/jp307091f.

56. R. Englman and J. Jortner, "The Energy Gap Law for Radiationless Transitions in Large Molecules," *Molecular Physics* 18, no. 2 (1970): 145–164, https://doi.org/10.1080/00268977000100171.

57. S. Upadhyayula, V. Nuñez, E. M. Espinoza, et al., "Photoinduced Dynamics of a Cyanine Dye: Parallel Pathways of Non-Radiative Deactivation Involving Multiple Excited-State Twisted Transients," *Chemical Science* 6 (2015): 2237–2251, https://doi.org/10.1039/C4SC02881C.

58. R. D. Pensack, A. J. Tilley, C. Grieco, et al., "Striking the Right Balance of Intermolecular Coupling for High-Efficiency Singlet Fission," *Chemical Science* 9, no. 29 (2018): 6240–6259, https://doi.org/10.1039/C8SC00293B.

59. M. W. B. Wilson, A. Rao, B. Ehrler, and R. H. Friend, "Singlet Exciton Fission in Polycrystalline Pentacene: From Photophysics Toward Devices," *Accounts of Chemical Research* 46, no. 6 (2013): 1330–1338, https://doi.org/10.1021/ar300345h.

60. W. Fudickar and T. Linker, "Why Triple Bonds Protect Acenes from Oxidation and Decomposition," *Journal of the American Chemical Society* 134, no. 36 (2012): 15071–15082, https://doi.org/10.1021/ja306056x.

61. A. Maliakal, K. Raghavachari, H. Katz, E. Chandross, and T. Siegrist, "Photochemical Stability of Pentacene and a Substituted Pentacene in Solution and in Thin Films," *Chemistry of Materials* 16, no. 24 (2004): 4980–4986, https://doi.org/10.1021/cm049060k.

62. L. Abu-Sen, J. J. Morrison, A. B. Horn, and S. G. Yeates, "Concentration- and Solvent-Dependent Photochemical Instability of 6,13-Bis(triisopropysilylethynyl)Pentacene," *Advanced Optical Materials* 2, no. 7 (2014): 636–640, https://doi.org/10.1002/adom.201400003.

63. K. J. Thorley, H. Le, Y. Song, and J. E. Anthony, "Unravelling the Major Factors in Photo-Oxidative Stability of Anthradithiophene Derivatives," *Journal of Materials Chemistry C* 10, no. 42 (2022): 15861–15871.

Supporting Information

Additional supporting information can be found online in the Supporting Information section.

Supporting File: adom71674-sup-0001-SuppMat.docx.